scientific reports

Check for updates

OPEN

Investigation of FGM patch repairs for cracked aluminum structures: J-integral analysis

Moulgada Abdelmadjid[1,2], Sahli Abderahmane[2], Zagane Mohammed El Sallah[1,2], Mordjani Ahmed[1], Adjoudj Tahar[1], Zafer Kurt[3]✉, Ecren Uzun Yaylacı[4] & Murat Yaylacı[3,5,6]

Functionally Graded Materials (FGMs) represent a highly advanced solution for the repair of cracked aircraft structures, offering superior performance compared to conventional homogeneous materials. FGMs contribute to more durable, lightweight, and structurally effective repairs, extending service life while maintaining safety and performance standards. This study investigates the effectiveness of functionally graded material (FGM) patches for reinforcing cracked aluminum alloy plates. Using three-dimensional finite element analysis implemented in ABAQUS with a USDFLD subroutine, spatial variations of the Young's modulus were applied according to linear, logarithmic, and exponential gradation laws. The fracture behavior was quantified through J-integral calculations under plane strain conditions. Results show that FGM patches significantly reduce the J-integral at the crack tip compared to unrepaired plates: up to 56% reduction for linear gradation, 52% for logarithmic, and 44% for exponential gradation. Linear gradation is most effective in mitigating longitudinal crack propagation, while logarithmic gradation efficiently reduces local principal stresses. Contour convergence and comparison with homogeneous patch and unrepaired plate benchmarks confirm the reliability of the numerical results. These findings provide mechanistic insight into stiffness-gradient-driven stress redistribution, guiding the optimal design of FGM repairs for enhanced durability.

Keywords FGM, Patch, Integral J, Stresses, Functions, USDFLD subroutine, Notch

Functionally graded materials (FGM's) have attracted attention in recent years due to their superior performance in areas such as improving stress distribution, enhancing crack performance, high fracture toughness and a high degree of design flexibility compared to traditional homogeneous materials[1–3]. Unlike traditional homogeneous materials[4,5], FGMs offer unlimited design architecture with their limitless variation options. Along with the attractive solutions they provide, they are the subject of researchers' work in all disciplines involving mechanics[6]. In addition, numerical methods such as semi-analytical methods[7], boundary element method[8] and finite element method[9–15] are available in the literature to obtain the changes created by the non-homogeneous structure of FGMs and the non-isotropic nature of the materials used. Khatir et al.[16] proposed a novel approach to optimize materials for middle ear prostheses in order to enhance auditory performance. A finite element (FE) model of the human ear incorporating a pure titanium total ossicular replacement prosthesis (TORP) was developed and validated against experimental data. Chama et al.[17] introduce a novel approach for reinforcing notched aluminum plates using functionally graded composites (FGCs). By incorporating the volume fraction principles of Functionally Graded Materials (FGMs) into fiber–matrix mixture laws, the study presents an advanced patch reinforcement strategy aimed at improving structural performance. Chama et al.[18] used a methodology leverages the volumetric fraction concept of Functionally Graded Materials (FGMs) to develop a Graded Cohesive Zone Model (GCZM). A spatially varying field, implemented via a Fortran-based USDFLD subroutine, is introduced to dynamically adapt the cohesive behavior of the interface within the GCZM framework. Izadi et al.[19] demonstrated that the comparison between experimental data and the derived fracture limit curve confirms the effectiveness of the newly developed criterion for analyzing mixed-mode fracture in functionally graded materials. Abdelmadjid et al.[20] concluded that stress distribution under varying loads shows a marked increase in intensity, particularly near the crack tip. This region, especially the upper part subjected to tensile forces,

[1]Department of mechanical engineering, Ibn Khaldoun University, BP 78 Zaaroura, 14000 Tiaret, Algeria. [2]Laboratory of Mechanics Physics of materials (LMPM), University Djillali Liabes Sidi Bel Abbes, 22000 Sidi Bel Abbès, Algeria. [3]Department of Civil Engineering, Recep Tayyip Erdogan University, 53100 Rize, Turkey. [4]Faculty of Fisheries, Recep Tayyip Erdogan University, 53100 Rize, Turkey. [5]Turgut Kıran Maritime Faculty, Recep Tayyip Erdogan University, 53900 Rize, Turkey. [6]Dijitalpark Teknokent, Murat Yaylacı-Luzeri R&D Engineering Company, 53100 Rize, Turkey. ✉email: zafer.kurt@erdogan.edu.tr

becomes highly stressed, potentially leading to crack initiation or opening and the development of significant localized stresses. Naderi et al.[21] reported that these variables significantly affect the fracture formation rate and overall fatigue life of the FGM. In particular, square-shaped Si_3N_4 particles demonstrated superior efficiency in arresting crack propagation compared to other geometries, owing to their ability to promote a more favorable stress distribution. Slamene et al.[22] employed a novel meshing technique in combination with the Gurson–Tvergaard–Needleman (GTN) damage model within ABAQUS/Explicit. The simulation, based on von Mises stress theory and the Voce hardening law, effectively captures plastic flow and progressive damage driven by void nucleation, growth, and coalescence. Kirk et al.[23] proposed a design methodology for planning FGM gradient paths across any number of elements, aiming to avoid undesirable phases over a range of temperatures. The methodology also enables optimization based on specific cost functions. A case study within the Fe–Ni–Cr system demonstrated its effectiveness, successfully generating gradient paths from 316 L stainless steel to pure chromium that either minimize path length or maximize the separation from unstable phases. Mirzaali et al.[24] investigated the fracture behavior of functionally graded soft hard composites containing a pre-existing crack aligned with the gradient direction. They designed, additively manufactured, and mechanically tested two primary types of FG composites those with step wise and continuous gradients. The results indicated that, with the exception of fracture strain, the fracture properties of the graded specimens generally decreased as the length of the transition zone increased. Kumar Singh et al.[25] presented a distinctive study in which a fully novel, in house developed manufacturing process was used to fabricate thermoplastic gears based on functionally graded materials (FGMs) a concept not previously explored. The specific wear rate of the fabricated gears was subsequently evaluated using the proposed methodology. Yaylaci et al.[26] examined a problem in which a functionally graded (FG) layer rests on a rigid foundation and is subjected to loading by a rigid punch. From the analysis, key parameters such as contact length, contact stress, initial separation distance, and the initiation and termination points of separation were determined and compared. The study concluded that the finite element method (FEM) results showed satisfactory agreement with the analytical solutions. Yaylaci et al.[27] assumed that the material properties of the functionally graded beam vary exponentially along its thickness. Using both the Finite Element Method (FEM) and the Modified Layerwise Plate (MLP) approach, they computed the natural frequencies and critical buckling loads of cracked FGM beams under various boundary conditions, including clamped–free (C–F), hinged–hinged (H–H), and clamped–clamped (C–C).This work aims to evaluate the effectiveness of functionally graded materials (FGM) in repairing cracked metallic components through numerical analysis using the ABAQUS software. Safaei[28] investigated the dynamic behavior of lightweight sandwich panels consisting of a polymeric foam core sandwiched between two composite surface layers, using a finite element method based on first-order shear deformation theory. In the study, different porosity distributions in the core (including uniform and functionally graded patterns) were considered, while the surface layers were modeled as fiber-reinforced laminates with various fiber orientations. Both free and forced vibration responses were analyzed to evaluate the effect of material and geometric parameters on overall structural performance. The results revealed that the vibration characteristics of the sandwich structure are significantly influenced by the porosity distribution in the core and the fiber orientation in the composite layers. Yang et al.[29] investigated the durability and structural stability of functionally graded graphene nanoparticle-reinforced composite beams at high temperatures using mathematical methods. Yang et al.[29] comprehensively analyzed the decisive effects of the distribution and geometry of graphene particles within the material on the structure's static and dynamic buckling resistance. Using the analytical model they developed, the deformation limits of the arch under sudden or constant external loads and its responses to temperature changes can be determined with high accuracy. Their results reveal how changes in the material's composition and thermal conditions transform the arch's load-bearing capacity, providing critical data for engineering designs.

The J integral generally refers to the Jacobi integral used in dynamical systems and clasic classical mechanics. It represents a conserved quantity in a rotating reference frame, combining the effects of energy and angular momentum. It is commonly used in analyses of the three-body problem. The J-integral has been widely employed in fracture mechanics, as well as in rigid line inclusion problems and frictionless contact analyses[30,31].

The study is based on analyzing stress distribution[32] and calculating key fracture resistance indicators such as the Von Mises equivalent stress, principal stress, J-integral, and displacement at the patch level, in order to assess the risk of crack propagation. The impact of three different property variation laws within the patch (linear, exponential, and logarithmic) is also examined, with the objective of determining which provides the most favorable stress distribution and the highest repair efficiency.

The novelty of the present work lies in three key aspects. First, a directional comparison of FGM gradation functions is performed by analyzing their effects on fracture parameters along the xxx, yyy, and zzz directions, providing deeper insight into how stiffness variation influences crack driving forces. Second, the study specifically focuses on unilateral FGM patch repair, which is less explored in the literature despite its practical relevance for real structural repairs. Third, the FGM patch is implemented through an anisotropic composite-based formulation using a USDFLD subroutine, allowing precise control of spatial stiffness variation and realistic representation of material gradation. These aspects have now been explicitly emphasized in both the Introduction and the Conclusion to clearly distinguish the present contribution from existing studies.

Material and method

Presentation of model

The geometric model studied consists of a thin rectangular plate made of 2024-T3 aluminum alloy, with a height H = 250 mm, a width L = 125 mm, and a thickness epl = 2 mm. This plate has a lateral crack located at one of its vertical edges, oriented horizontally, and positioned perpendicular to the direction of the applied load, along the y-axis. The crack, of length a = 8 mm. To remedy this damage, a single reinforcement plate (patch) made of functionally graded material (FGM) is applied to a single face of the plate, precisely on the side where the

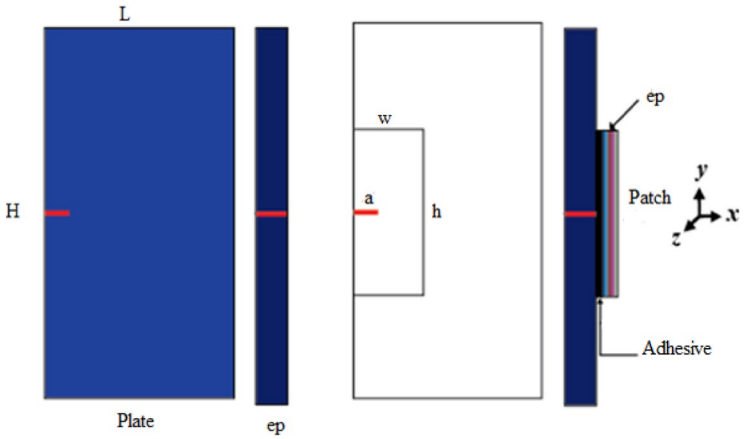


Fig. 1. Geometric model.

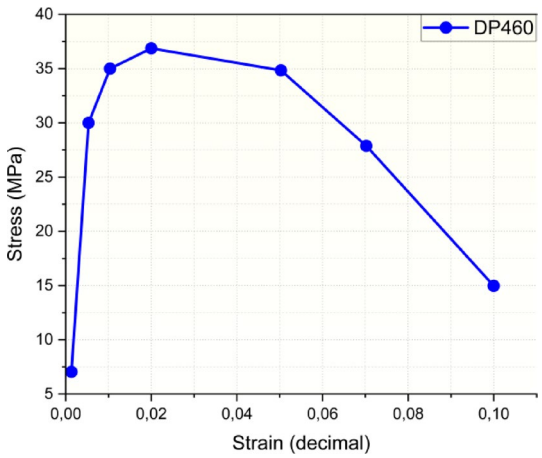


Fig. 2. Stress-strain curve of DP 460 adhesive[35].

crack is located. This patch has a height of h = 50 mm, a width of w = 25 mm and a thickness of ep = 1 mm. The adhesion between the plate and the patch is ensured by a layer of glue with a thickness of ec = 0.2 mm, allowing good transmission of mechanical forces and effective anchoring of the reinforcement. The assembly is subjected to a uni-axial tensile loading along the vertical axis (y), with a stress of 30 MPa. This configuration aims to analyze the influence of unilateral repair using an FGM patch on the reduction of stress concentration near the crack, and to evaluate the overall mechanical performance of the repaired plate as a function of the gradient of properties of the patch material. (see Fig. 1).

Material properties

The thin plate is assumed to be manufactured from 2024-T3 aluminium alloy and possesses isotropic material properties. In addition, its mechanical properties can be defined by its Young's modulus (E_p = 69 GPa) and Poisson's ratio (ν = 0.33), respectively.

The adhesive used to bond the plate to the patch is DP460[33,34], a material frequently used in aerospace applications, and its stress-strain relationship is shown in Fig. 2. It is also assumed to possess isotropic material properties, and it is assumed to have the following values: Young's Modulus (E) = 1300 MPa, Poisson's ratio (ν) = 0.3.

It is assumed that the patch plate to be used for improving stresses on the crack using functionally graded material (FGM) consists of two different types of material and has anisotropic properties. The values required for defining the material based on the two different material types and anisotropy are given in Table 1.

The functionally graded material (FGM) patch is modeled by spatially varying the *Young's modulus only*, while Poisson's ratio and density are assumed constant. This assumption is commonly adopted in FGM repair studies and allows isolation of the effect of stiffness gradation on crack driving forces. The elastic modulus is graded according to a prescribed analytical law (linear, logarithmic, or exponential) as a function of spatial coordinates, implemented via the *USDFLD subroutie in ABAQUS*[38]. The material behavior remains isotropic

Materials	E_1 (GPa)	E_2 (GPa)	E_3 (GPa)	ν_{12}	ν_{13}	ν_{23}	G_{12}	G_{13}	G_{23}
Boron/Epoxy	202	31	31	0.26	0.26	0.1	8061	8061	1400
Glass/Epoxy	25	3,050	3,050	0.35	0.35	0.38	801	801	470

Table 1. Mechanical properties of patch[36,37].

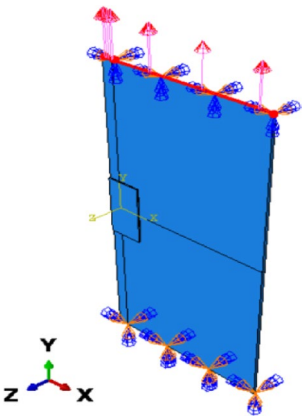


Fig. 3. Presentation of the model with boundary conditions.

at each material point, and therefore all stiffness components are derived consistently from the local Young's modulus and constant Poisson's ratio.

Since isotropy is assumed, no preferential anisotropic axes are defined, and the material orientation is independent of the crack direction. The gradation direction is aligned with the patch geometry and crack plane to ensure effective stress redistribution around the crack tip. A schematic description and a brief pseudo-code explanation of the USDFLD implementation have.

been added to improve clarity and reproducibility.

Boundary conditions and loading

Regarding the boundary conditions, the embedding of the lower face of the plate is applied by fixing all the components of the displacements: U1 = U2 = U3 = 0 (displacements in X, Y and Z) and UR1 = UR2 = UR3 = 0 (rotations around the X, Y and Z axes). This represents a rigid support condition at this face, preventing any movement (see Fig. 3).

Side of the plate, a uni-axial tensile stress of 30 MPa is applied, generating a mechanical stress on the cross-section of the plate. This configuration allows the analysis of the behavior of the plate in response to these loading conditions, taking into account the FGM patch repair.

Theoretical background

This work is based on a rigorous simulation, implemented in ABAQUS software, using a custom subroutine (notably USDFLD coded in FORTRAN) to implement the spatial variations of the mechanical properties in the patch. The different functions used in the subroutines are (the linear, exponential and logarithmic function) presented with the equations cited below.

Linear function $E(x) = E_{\max} - (E_{\max} - E_{\min}) \cdot \frac{x}{L}$

Exponential function $E(y) = E_{max} \cdot e^{-ky}$

Logarithmic function $E(z) = E_{\min} + (E_{\max} - E_{\min}) \frac{\mathrm{In}\left(1+k\frac{z}{h}\right)}{\mathrm{In}(1+k)}$

E (z): Young's modulus at position z.

Emin: Young's modulus at the metal-rich side of the FGM patch.

Emax: Young's modulus at the ceramic-rich side of the FGM patch.

z: thickness coordinate ($0 \le z \le h$).

h: total thickness of the FGM patch.

The fracture analysis was performed within the framework of linear elastic fracture mechanics under plane strain conditions, which is appropriate for the considered aluminum plate thickness and crack dimensions. The J-integral was evaluated in ABAQUS using the domain-based integral formulation, with (05) five successive contours defined around each crack tip. For all analyzed cases and material gradation functions, the J-integral values showed excellent contour convergence, confirming the path independence of the integral and the numerical stability of the results (see Fig. 4). In particular, the convergence behavior was verified for the different FGM gradation laws (linear, logarithmic, and exponential), demonstrating that the observed variations in

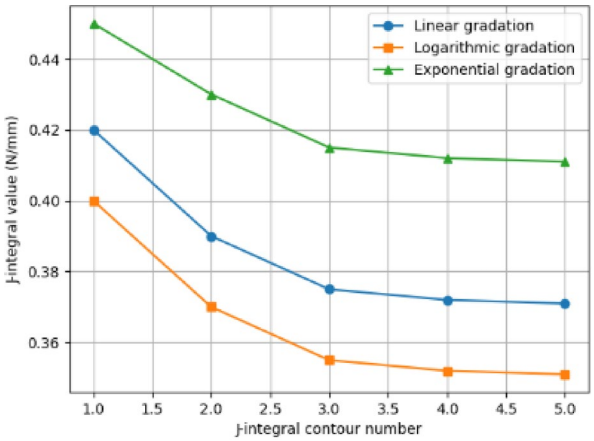


Fig. 4. the J-integral convergence for different FGM graduation functions.

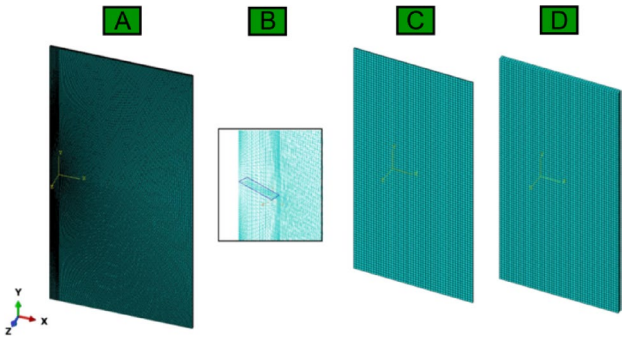


Fig. 5. Presentation of the geometric model mesh (**A**) Plate, (**B**) Crack, (**C**) Adhesive (**D**) FGM patch.

Element	Number of elements	Number of nodes	Type of elements
Plate	138,240	174,840	C3D8R
Adhesive	4608	9506	C3D8R
Patch	10,000	15,453	SC8R

Table 2. Number of nodes and elements of the parts.

J-integral are attributable to material gradation effects rather than numerical artifacts. This ensures the reliability of the conclusions regarding the influence of Young's modulus distribution on crack driving forces and repair efficiency.

Mesh

In the system modeling, two types of elements are used to represent the plate and its mechanical characteristics under stress. Linear hexahedral elements of the C3D8R type (3D solid element with 8 nodes and reduced integration) are used for the plate and the same for the adhesive layer. In addition, SC8R elements (continuous shell element with 8 nodes and reduced integration) are used to model the FGM patch (see Fig. 5) The element types, number of node and elements used in the analyses are presented in Table 2.

Results and discussions

For the variation of the patch in FGM, we stress the plate of a patch with a maximum Young's modulus at the interface (plate/patch) and a minimum Young's modulus on the free side of the patch, and see the different results emerging from this simulation. This choice aims to optimize the redistribution of stresses and to minimize mechanical incompatibilities at the interfaces. The simulation allows observing the effects of this graduated variation on several aspects, such as, the reduction of the stress peak near the crack, as well as the evolution of the J integral, an energy indicator of the potential propagation of the crack.

The variation of FV1 in the FGM patch

Each Young's modulus variation function applied in the FGM patch models a distinct scenario of stiffness distribution across the material. In this context, the field variable denoted FV (Field Variable), used to control the field-dependent material behavior, takes normalized values between zero (0) and one (1). When FV = 0, this corresponds to the area closest to the crack, where the stiffness (Young's modulus) is maximal, ensuring targeted mechanical reinforcement. Conversely, when FV = 1, the periphery of the patch is reached, where stiffness is minimal, promoting better compatibility with the surrounding structure and limiting stress concentrations at the interfaces. This approach thus makes it possible to grade the mechanical properties of the patch to optimize force distribution and reduce mechanical discontinuities. The images obtained for the different simulations tested are shown in Fig. 6.

Variation of the Von Mises stress in the FGM patch

For the variation of the Von Mises stress in the FGM patch, each function presents a model of distribution of the stresses, and according to the axis under study and for different values, and this translates the effect of the evolution of the different properties of the patch in FGM following the function used. Figure 7 depicts the variation of Von Mises stresses on geometric model for three different gradation functions. Also, Fig. 8 demonstrates Von misses stress values for linear, logaritmic and exponancial gradation functions.

The variation of Von Mises stresses in the FGM patch directly reflects the influence of the gradation profile of mechanical properties imposed by each Young's modulus variation function. Each adopted function (linear or exponential) defines a distinct stress distribution pattern along a given axis, and for different values of the variation field. This distribution strongly depends on how the stiffness evolves inside the patch, influencing the latter's ability to redistribute forces around the crack. Among the functions studied, it is particularly notable that the exponential function along the z-axis allows achieving the lowest Von Mises stress, with a minimum value of about 16.1 MPa, indicating an excellent capacity for mitigating localized stresses thanks to a smooth transition of mechanical properties in the thickness of the patch.

On observe that the exponential and logarithmic functions applied along the z-axis induce relatively low Von Mises stresses compared to the other variation laws, which underlines their effectiveness in grading stiffness across the patch thickness in a progressive and smooth manner. This vertical gradation allows for better stress dissipation and limits stress peaks around the crack. Furthermore, the linear function along the (x) axis also exhibits lower Von Mises stresses, but to a lesser extent compared to the exponential and logarithmic functions along z. This suggests that the distribution of mechanical properties in the longitudinal (x) direction also contributes to stress mitigation, although less effectively than a gradation across the thickness. Overall, these results highlight the importance of the choice of the variation law and its orientation in the optimal design of FGM patches.

Analysis of maximum principal stresses

The different stress distributions, it is necessary to rely on the main maximum stress, which clearly shows the stress distribution at the patch level for the different FGM functions at the plate/patch interface. Figure 9 illustrates the maximum principal stress distributions formed in the models for three different rating functions.

The analysis of the principal stresses in the three directions (x, y, z) highlights the significant influence of the type of variation function used in the FGM patch. In the (x) axis, the linear function generates the lowest stresses, reaching 20.35 MPa, with relaxation in the vicinity of the crack, which reflects a good redistribution of forces. It is followed by the logarithmic function (approximately 26.5 MPa) and then by the exponential function (41.6 MPa), which presents higher stresses in this direction. On the other hand, in the y axis (direction of the stress), it is the exponential function that is distinguished by the lowest stresses, of the order of 14 MPa, with a localized concentration at the crack tip followed by an extended relaxation in the rest of the patch. Finally, in the z-axis (thickness), the exponential function continues to show excellent performance with stresses reduced to 10.4 MPa, and a very limited concentration at the crack tip. Beyond this zone, the effect of stresses becomes almost weak, reflecting an excellent capacity for absorption and diffusion of forces through the thickness. These results confirm that the judicious choice of the FGM function according to the direction can significantly improve the mechanical performance of the patch, by reducing stress concentrations and extending the lifetime of the repaired structure.

The variation of displacement in the FGM patch

Concerning the displacements induced in the FGM patch, the analysis focused on the U2 displacement, which corresponds to the displacement along the (y) axis, i.e. in the direction of the applied stress (traction). The results show that, whatever the variation function used (linear, exponential, and logarithmic) and whatever the axis considered (x, y or z), the displacements remain globally similar, with values between 0.061 mm and 0.065 mm. This low variation indicates that, despite the differences in Young's modulus gradation in the patch, the overall effect on the longitudinal deformation of the plate remains moderate. This suggests that the main role of the different FGM functions is not to significantly modify the overall flexibility of the system, but rather to reduce local stress concentrations without altering the overall displacement response under loading. The displacement change in different axes for different functions is shown in Fig. 10. The change in displacement values occurring along the axes and the displacement effect created by the gradation function on the model along different axes can be examined in the graph in Fig. 11.

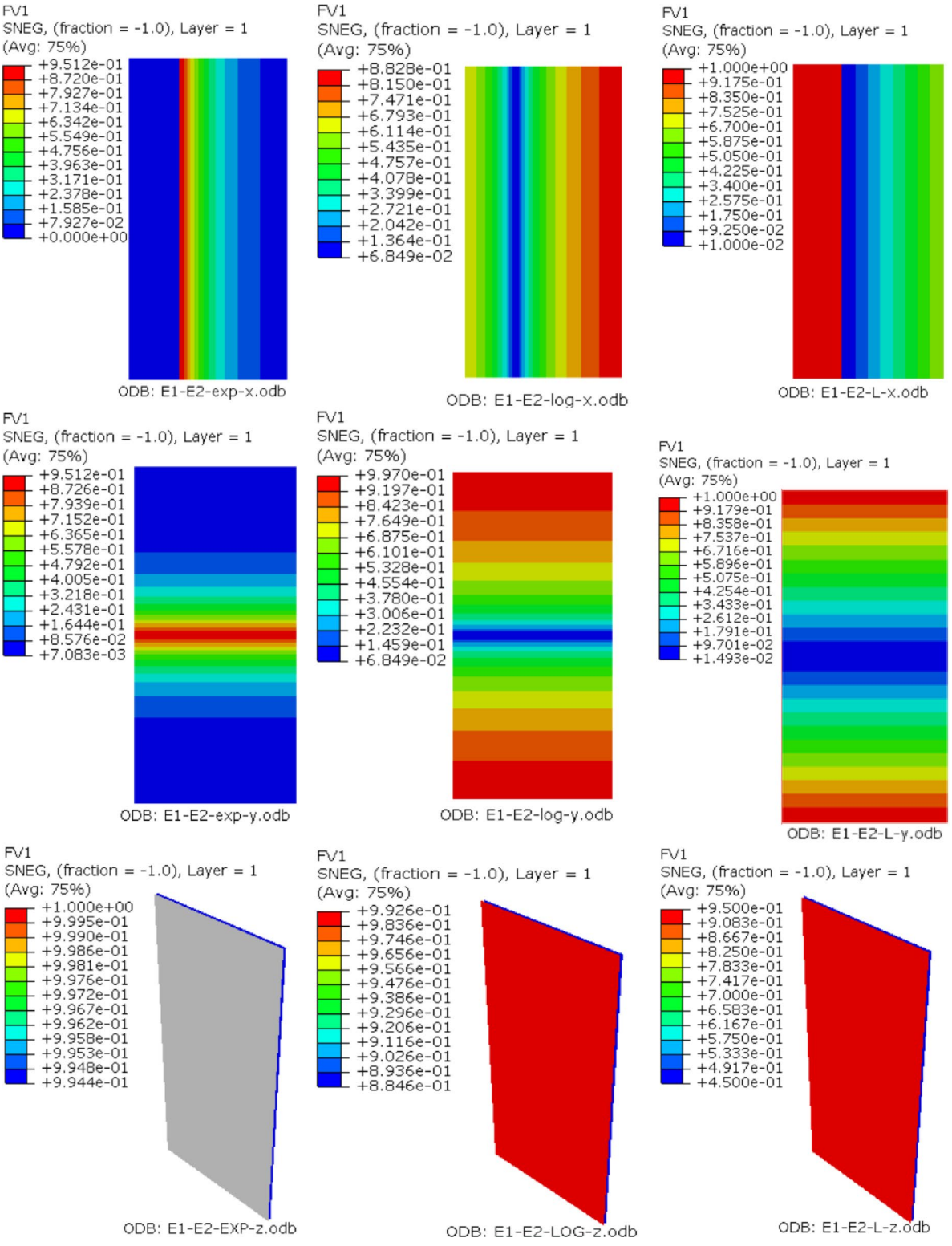


Fig. 6. Presentation of the different variation functions tested.

Analysis of the variation of the J-integral in the repaired plate

a) For the variation of the patch along the (x) axis

The Fig. 12 illustrates the variation of the J-integral as a function of the normalized distance in the plate repaired using different FGM patches along the x-axis, highlighting the significant impact of the nature of the stiffness gradient on the resistance to crack propagation. It is clear that the exponential function generates the lowest values of the J-integral, especially at the plate/patch interface, where it reaches about 0.14 J/mm^2. This is

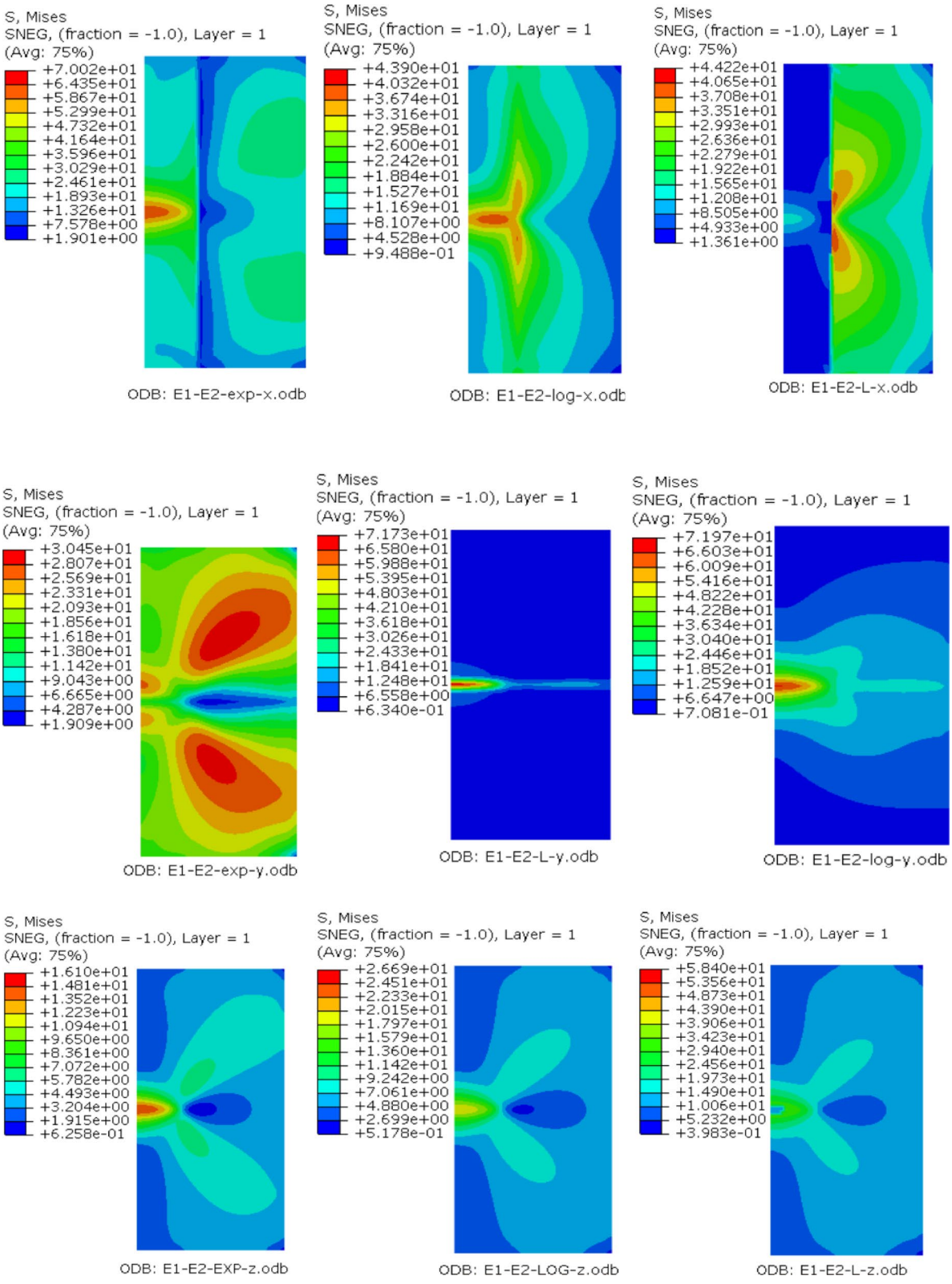


Fig. 7. Distribution of von mises stress for each function.

followed by the logarithmic function with a value of about 0.18 J/mm², and then by the linear function, which remains slightly higher. In comparison, the unrepaired plate shows significantly higher values, exceeding 0.36 J/mm², which confirms the beneficial effect of the FGM patches. These results show that the addition of a patch, particularly with an exponential variation of the mechanical properties, makes it possible to considerably reduce

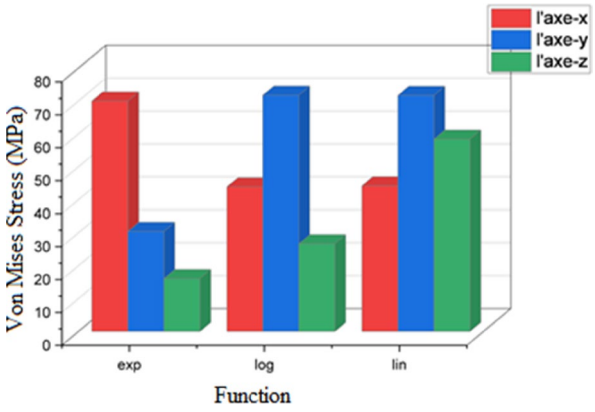


Fig. 8. Evolution of von mises stress for different functions.

the fracture energy (J-integral) and therefore to effectively slow down crack propagation, particularly at the critical level of the interface between the plate and the patch.

b) For the variation of the patch along the (y) axis
In Fig. 13, on observe that the logarithmic function applied to the FGM patch generates the lowest values of the J-integral compared to the exponential and linear functions, with values that do not exceed 0.23 J/mm². This performance indicates a better efficiency in terms of resistance to crack propagation, especially in the critical zone close to the crack tip. All the results highlight that the use of an FGM patch, regardless of the variation profile, allows to significantly reducing the J-integral compared to the unrepaired plate. This behavior is particularly notable at the plate/patch interface, where the effect of the patch is manifested by stress absorption and effective relaxation of the stress field around the crack. Thus, the FGM acts not only as a structural reinforcement, but also as a mechanical modulator that attenuates local singularities, improving the durability and safety of the repaired structure.

c) For the variation of the patch along the (z) axis
The variation of J-integral values along the z-axis is displayed in Fig. 14 for cracks that have not been repaired, cracks repaired with plates, and for three different rating functions. For the variation of the J-integral as a function of the normalized distance in the plate repaired with different FGM patches along the z-axis (thickness), it is clearly observed that the linear function generates the lowest values of the J-integral, reflecting a good capacity to mitigate the fracture energy. It is followed by the logarithmic function, then by the exponential function, which presents a value of approximately 0.18 J/mm² at the plate/patch interface. Although the three functions present slightly different performances, they all have in common to produce values significantly lower than those obtained for the unrepaired plate, where the J-integral exceeds 0.38 J/mm². This highlights the beneficial effect of the FGM patch, especially when optimized according to the plate thickness, to significantly reduce the crack propagation energy. The stiffness gradient in the (z) direction allows a gradual transition of mechanical properties, thus minimizing stress concentrations and providing better relaxation at the crack.

d) For the variation of the patch along the three axis (x, y and z)
The analysis of the J-integral variation as a function of the normalized distance in the repaired plate for different FGM patches, along the x, y, and z-axes, reveals clear trends in terms of mechanical efficiency (see Fig. 15) The exponential function along the x-axis is distinguished by the lowest J-integral values, especially at the plate/patch interface, which reflects an excellent ability to mitigate crack propagation energy in this configuration. It is closely followed by the logarithmic function, which also shows reduced J-integral values along all axes (x, y, z), both at the plate/patch interface and at the free edge of the plate. These results highlight the effectiveness of the exponential and logarithmic variation functions in the design of FGM patches to limit energy concentration effects, thus contributing to a more durable and secure repair of the cracked structure.

To validate the proposed numerical approach, benchmark comparisons were performed against an unrepaired cracked plate and a homogeneous patch limit case. The unrepaired configuration exhibits the highest J-integral value (0.48 N/mm), serving as a reference baseline. The introduction of a homogeneous patch reduces the J-integral by approximately 38%, while FGM patches provide significantly greater reductions, reaching up to 56% for the linear gradation law (Table 3). These results clearly demonstrate the added benefit of stiffness gradation over conventional homogeneous repairs and are consistent with trends reported in previous numerical studies, thereby reinforcing the credibility of the present model.

Conclusion

This study emphasizes the significance of functionally graded materials (FGMs) as advanced and effective solutions for crack repair in structural components, particularly those made of aluminum alloys. The numerical analysis carried out using ABAQUS demonstrated the effectiveness of FGM patches in enhancing the mechanical performance of cracked structures by reducing the J-integral and distributing stresses more

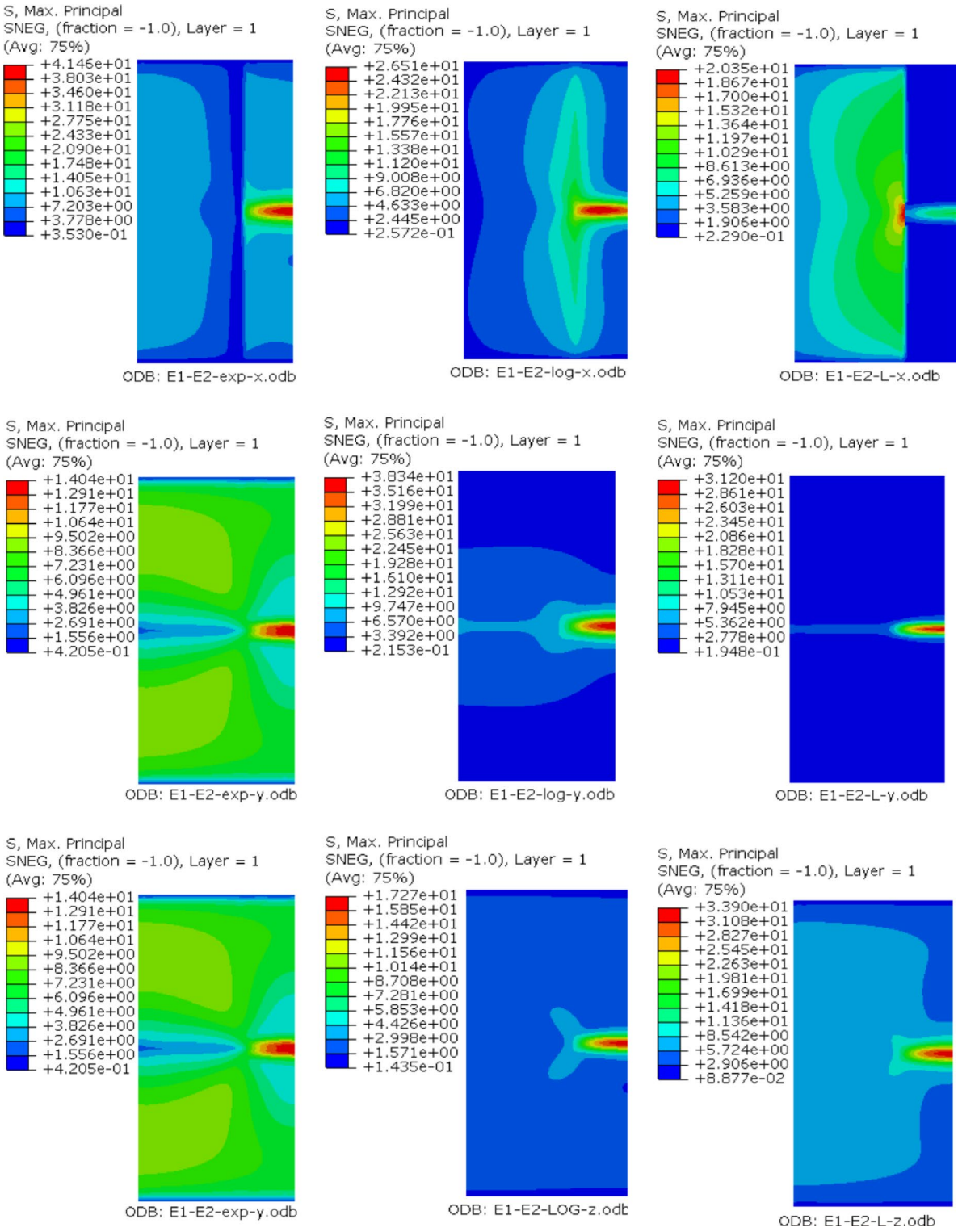


Fig. 9. Distribution of different maximum principal stresses in the patch for different functions.

uniformly around crack tips The effectiveness of the patch depends on several factors, including its thickness, the quality of its adhesion to the surface, and its geometric distribution around the crack. All of these criteria play a significant role in enhancing structural durability and reducing the risk of crack propagation. The comparison of different gradation functions (exponential, logarithmic, and linear) also revealed a clear influence of each on the structural response, highlighting the importance of selecting the most appropriate function based on the specific application requirements.

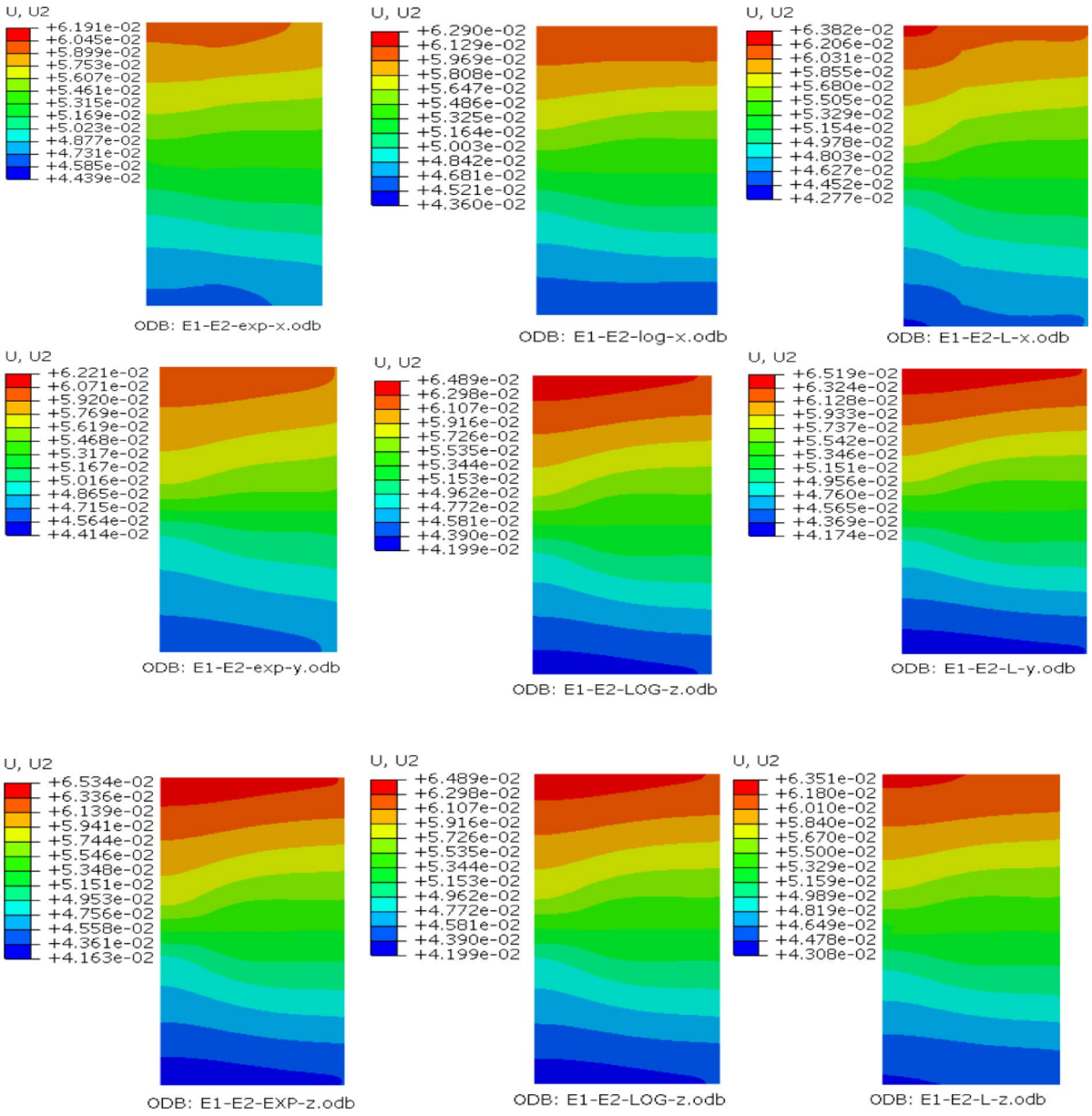


Fig. 10. Variation of different displacements for different functions.

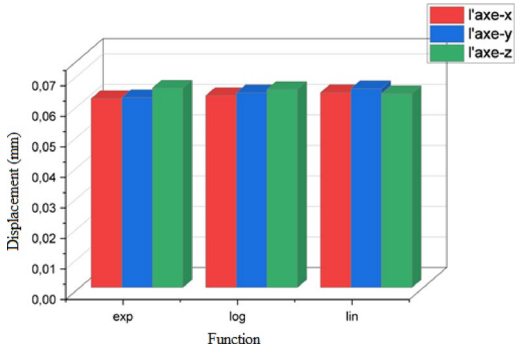


Fig. 11. Variation of displacements for different functions.

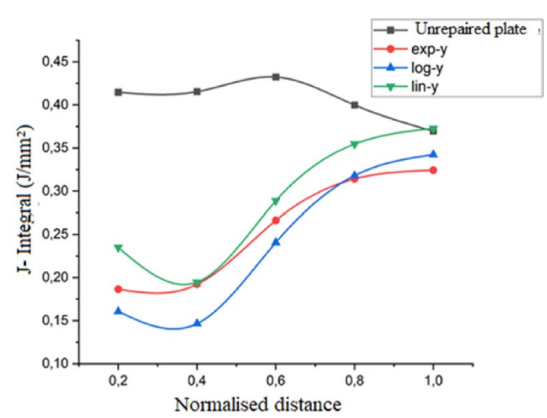


Fig. 12. Variation of the J-integral as a function of the normalized distance in the repaired plaque for different FGM patches (along the x-axis).

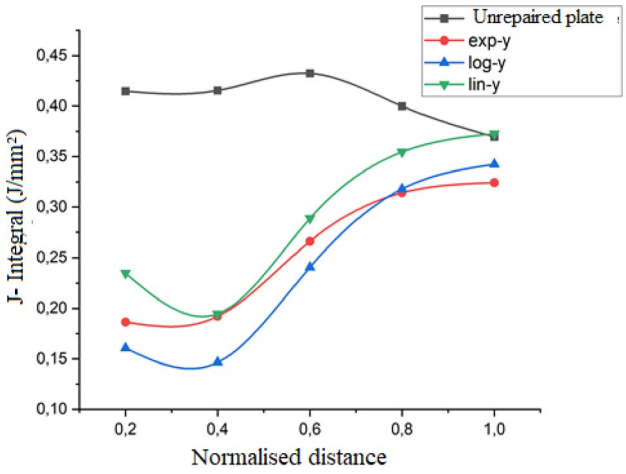


Fig. 13. Variation of the J-integral as a function of the normalized distance in the repaired plaque for different FGM patches (along the y-axis).

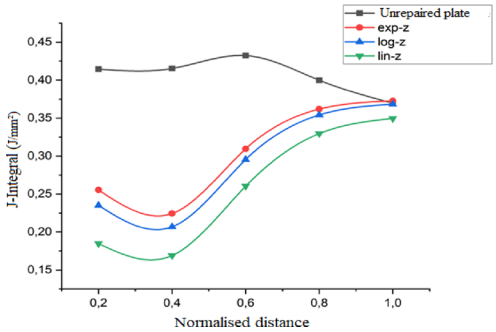


Fig. 14. Variation of the J-integral as a function of the normalized distance in the repaired plaque for different FGM patches (along the z-axis).

The study of variations in the J-integral and maximum principal stresses for different FGM patches reveals that the gradation function of the Young's modulus plays a key role in the mechanical effectiveness of the reinforcement. Overall, the linear function stands out for its ability to reduce the J-integral in both the x and y directions, while the logarithmic function proves particularly effective in limiting principal stresses in specific regions and facilitating stress relaxation near the crack.

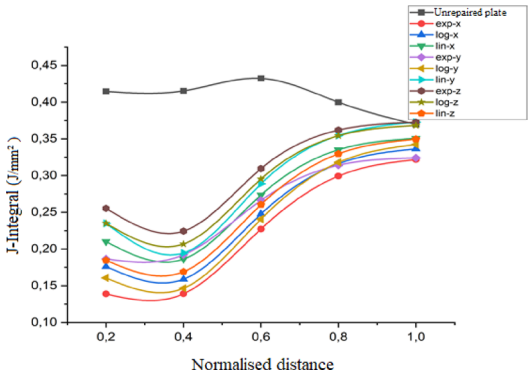


Fig. 15. Variation of the J-integral as a function of the normalized distance in the repaired plaque for different FGM patches (along the x, y, z-axes).

Configuration	Patch type	Maximum J-integral (*N*/mm)	Reduction vs. unrepaired (%)
Unrepaired cracked plate	—	0.48	—
Repaired plate	Homogeneous patch	0.30	37.5
Repaired plate	FGM patch – exponential	0.27	43.8
Repaired plate	FGM patch – logarithmic	0.23	52.1
Repaired plate	FGM patch – linear	0.21	56.3

Table 3. Benchmark comparison of fracture parameters.

However, the exponential function, while effective at absorbing stresses through the patch thickness in the z-direction, shows higher J-integral values in the x-direction, indicating a more limited capacity to dissipate crack propagation energy in that direction. These results confirm the importance of carefully selecting the gradation function to optimize stress redistribution, reduce stress concentrations, and ultimately improve the overall performance of FGM patch repairs.

These results highlight that the choice of the Young's modulus gradation function significantly influences the distribution of the J-integral in different directions. In particular, while the exponential function is effective in the z-direction for reducing through-thickness stresses, it exhibits higher values in the x-direction, which may be less favorable for controlling longitudinal crack propagation. These observations emphasize the importance of tailoring the Young's modulus gradation to the dominant loading conditions in order to optimize the performance of FGM patches and thereby enhance the durability and safety of cracked plate repairs.

Data availability

The data that support the findings of this study are available on request from the authors.

Received: 23 March 2026; Accepted: 8 May 2026
Published online: 19 May 2026

References

1. Meski, K. et al. Elastic instability of functionally graded sandwich plates with auxetic honeycomb core subjected to thermal and magnetic fields. *Int. J. Struct. Stab. Dyn.* 2650272. https://doi.org/10.1142/S021945542650272X (2025).
2. Wang, Z., Zhou, Y., Brahmia, A. & Jastaneyah, Z. Investigating aerothermodynamic characteristics of environmentally friendly materials in composite plates embedded in a Kerr-Type foundation using mathematics formulation and artificial intelligence techniques. *Int. J. Struct. Stab. Dyn.* 2650305. https://doi.org/10.1142/S0219455426503050 (2025).
3. Nešić, N., Cajić, M., Karličić, D., Lazarević, M. & Adhikari, S. Vibration and stability of a nonlinear nonlocal strain-gradient FG beam on a visco-Pasternak foundation. *Facta Univ. Ser. Mech. Eng.* **23** (4), 709–733. https://doi.org/10.22190/FUME230419022N (2025).
4. Abouelregal, A. E. et al. The dual phase lag model for thermoelastic microbeams embedded in an elastic foundation incorporating fractional Kelvin–Voigt viscoelasticity. *Mech. Mater.* **205**, 105336. https://doi.org/10.1016/j.mechmat.2025.105336 (2025).
5. Ghanati, P. & Safaei, B. Elastic buckling analysis of polygonal thin sheets under compression: P Ghanati and B Safaei. *Indian J. Phys.* **93** (1), 47–52. https://doi.org/10.1007/s12648-018-1254-9 (2019).
6. Garai, R., Gartia, A. K. & Chakraverty, S. Effect of Axial Functional Gradation and Periodic Square Perforations on the Vibration of Nanobeams with Elastic Foundation. *Int. J. Struct. Stab. Dyn.* 2750188. https://doi.org/10.1142/S0219455427501884 (2026).
7. Sun, T., Wang, F. & Yue, X. A novel local semi-analytical meshless method for acoustic eigenfrequency and modal analysis. *Appl. Math. Lett.* 109854. https://doi.org/10.1016/j.aml.2025.109854 (2025).
8. Han, X. et al. A semi-analytical method for vibration and buckling analysis of composite laminated cylindrical shells under external hydrostatic pressure. *Int. J. Struct. Stab. Dyn.* 2650274. https://doi.org/10.1142/S0219455426502743 (2025).
9. Turna, I. et al. Allision risk and impact analysis in recreational fishing boats using fuzzy bayesian networks and the finite element method. *Fish. Res.* **291**, 107544. https://doi.org/10.1016/j.fishres.2025.107544 (2025).

10. Öztürk, O. B. et al. An integrated interval type-2 fuzzy SLIM and FEM model for working aloft risk analysis in shipboard operations. *Appl. Ocean Res.* **163**, 104742. https://doi.org/10.1016/j.apor.2025.104742 (2025).
11. Ammarullah, M. I. et al. Influence of radial clearance on Tresca stress in Al_2O_2-on-Al_2O_3 bearings for total hip prosthesis evaluated using finite element analysis. *Sci. Rep.* **15** (1), 33091. https://doi.org/10.1038/s41598-025-16850-4 (2025).
12. Ammarullah, M. I. Integrating finite element analysis in total hip arthroplasty for childhood hip disorders: Enhancing precision and outcomes. *World J. Orthop.* **16** (1), 98871. https://doi.org/10.5312/wjo.v16.i1.98871 (2025).
13. Ammarullah, M. I. et al. Computational prediction of running-in wear in hard-on-hard dual mobility total hip prostheses during the gait cycle. *Proc. Inst. Mech. Eng. Part. J: J. Eng. Tribol.* https://doi.org/10.1177/13506501261416l9 (2026).
14. Ammarullah, M. I. et al. Finite element-based wear prediction using archard's law for single mobility bearing of total hip prosthesis during walking. *Lit. Rev. Eng. Rep.* **8** (2), e70628. https://doi.org/10.1002/eng2.70628 (2026).
15. Ammarullah, M. I. et al. Minimizing risk of failure from ceramic-on-ceramic total hip prosthesis by selecting ceramic materials based on tresca stress. *Sustainability* **14** (20), 13413. https://doi.org/10.3390/su142013413 (2022).
16. Khatir, O. et al. Optimizing mechanical behavior of middle ear prosthesis using finite element method with material degradation FGM in three functions. *Mech. Adv. Mater. Struct.* **32** (3), 478–487. https://doi.org/10.1080/15376494.2024.2350677 (2025).
17. Chama, M., Moulai-Khatir, D., Hamza, B., Slamene, A. & Mokhtari, M. Advanced damage prediction in notched plates reinforced with Graded composite patches: Integrating XFEM-CZM and fiber-matrix coupling laws using functionally graded materials. *Mech. Adv. Mater. Struct.* **32** (13), 2998–3015. https://doi.org/10.1080/15376494.2024.2387741 (2025).
18. Chama, M., Moulai-Khatir, D., Hamza, B., Slamene, A. & Mokhtari, M. Novel FGM-USDFLD approach in Graded Cohesive Zone Modeling (GCZM): Predicting debonding and crack propagation in composite-patched notched plates. *Mech. Adv. Mater. Struct.* **32** (13), 3144–3159. https://doi.org/10.1080/15376494.2024.2389451 (2025).
19. Izadi, S. M. H., Fakoor, M. & Mirzavand, B. Developing a new mixed mode I/II fracture criterion for cracked functionally graded materials considering the fracture process zone effect. *Acta Mech.* **236** (1), 21–35. https://doi.org/10.1007/s00707-024-04136-1 (2025).
20. Abdelmadjid, M. et al. Effects of the stiffness of an inclusion on the mechanical behavior of an aluminum alloy plate with a lateral notch. *Steel Compos. Struct.* **51** (1), 63–72. https://doi.org/10.12989/scs.2024.51.1.063 (2024).
21. Naderi, E., Taghizadeh, M. & Alinia, Y. An extended finite element method study on the effect of reinforcing particles on the fatigue crack propagation behavior of functionally graded plates. *AUT J. Mech. Eng.* **9** (3), 295–316. https://doi.org/10.22060/ajme.2025.23786.6155 (2025).
22. Slamene, A. et al. Assessing gradient parameters for damage control in notched plates: Finite element analysis of locally functionally graded materials using the Gurson-Tvergaard-needleman (GTN) model. *Mech. Based Des. Struct. Mach.* **53** (2), 1392–1428. https://doi.org/10.1080/15397734.2024.2385025 (2025).
23. Kirk, T., Galvan, E., Malak, R. & Arroyave, R. Computational design of gradient paths in additively manufactured functionally graded materials. *J. Mech. Des.* **140** (11). https://doi.org/10.1115/1.4040816 (2018).
24. Mirzaali, M. J. et al. Fracture behavior of bio-inspired functionally graded soft–hard composites made by multi-material 3D printing: the case of colinear cracks. *Materials* **12** (17), 2735. https://doi.org/10.3390/ma12172735 (2019).
25. Kumar Singh, A. Thermal and wear behavior of glass fiber-filled functionally graded material-based polyamide 66 spur gears manufactured by a novel technique. *J. Tribol.* **140** (2), 021601. https://doi.org/10.1115/1.4037335 (2018).
26. Yaylacı, M. et al. Analyzing of continuous and discontinuous contact problems of a functionally graded layer: theory of elasticity and finite element method. *Mech. Based Des. Struct. Mach.* **52** (8), 5720–5738. https://doi.org/10.1080/15397734.2023.2262562 (2024).
27. Yaylacı, M., Yaylacı, E. U., Özdemir, M. E., Öztürk, Ş. & Sesli, H. Vibration and buckling analyses of FGM beam with edge crack: Finite element and multilayer perceptron methods. *Steel Compos. Struct. Int. J.* **46** (4), 565–575. https://doi.org/10.12989/scs.2023.46.4.565 (2023).
28. Safaei, B. Frequency-dependent damped vibrations of multifunctional foam plates sandwiched and integrated by composite faces. *Eur. Phys. J. Plus*. **136** (6), 646. https://doi.org/10.1140/epjp/s13360-021-01632-4 (2021).
29. Yang, Z. et al. Thermally induced instability on asymmetric buckling analysis of pinned-fixed FG-GPLRC arches. *Eng. Struct.* **250**, 113243. https://doi.org/10.1016/j.engstruct.2021.113243 (2022).
30. Borisov, A. V., Mamaev, I. S. & Bizyaev, I. A. The Jacobi integral in nonholonomic mechanics. *Regul. Chaotic Dyn*. **20** (3), 383–400. https://doi.org/10.1134/s1560354715030107 (2015).
31. Ma, Z. Y. & Huang, G. Y. Application of J-integral to adhesive contact under general plane loading for rolling resistance. *Appl. Math. Model.* **137**, 115700. https://doi.org/10.1016/j.apm.2024.115700 (2025).
32. Ammarullah, M. I. et al. A review of enhanced total hip prosthesis design and material bearing combination to accommodate Muslim prayer (Salat) movements: Biomechanical, biotribological, and biological perspectives. *Tribol. Int.* **205**, 110518. https://doi.org/10.1016/j.triboint.2025.110518 (2025).
33. He, H., Forouzan, F., Volpp, J., Robertson, S. M. & Vuorinen, E. Microstructure and mechanical properties of laser-welded DP steels used in the automotive industry. *Materials* **14** (2), 456. https://doi.org/10.3390/ma14020456 (2021).
34. Abdelhussien, A. et al. Analysis of the mechanical characteristics of date seed powder-based composite carbon fiber reinforced polymers. *Facta Universitatis Series: Mech. Eng.* **23** (2), 251–263. https://doi.org/10.22190/FUME230728040A (2025).
35. Banea, M. D. & da Silva, L. F. Adhesively bonded joints in composite materials: an overview. *Proc. Inst. Mech. Eng. Part L: J. Mater. Des. Appl.* **223** (1), 1–18. https://doi.org/10.1243/14644207JMDA219 (2009).
36. Gay, D., Hoa, S. V. & Tsai, S. W. *Composite Materials: Design and Applications* 1st edn, (CRC, 2002). https://doi.org/10.1201/9781420031683.
37. Mallick, P. K. *Fiber-Reinforced Composites: Materials, Manufacturing, and Design*. 638. (CRC Press, 2007). https://doi.org/10.1201/9781420005981.
38. ABAQUS. ABAQUS/Standard: User's Manual, Dassault Systèmes Simulia, Johnston, RI. (2017).

Author contributions

Moulgada Abdelmadjid Writing – original draft Conceptualization Validation. Sahli Abderahmane Writing – original draft Data curation Software. Zagane Mohammed El Sallah Writing – original draft Project administration Data curation. Mordjani Ahmed Writing – original draft Investigation Software. Adjoudj Tahar Writing – original draft Formal analysis Validation. Zafer kurt Writing – review & editing, Visualization. Ecren uzun yaylacı Writing – review & editing, Visualization. Murat Yaylacı Writing – review & editing, Supervision.

Declarations

Competing interests

The authors declare no competing interests.

Ethical approval
The authors declare that the research was conducted according to ethical standards. This article does not contain any studies with human or animal subjects.

Consent to participate
No external participants have contributed to the work discussed in this manuscript.

Consent for publication
The authors give their full consent to the editor to publish this article if accepted. Authors confirmed not use of AI and AI-assisted technologies in the writing process.

Additional information
Correspondence and requests for materials should be addressed to Z.K.

Reprints and permissions information is available at www.nature.com/reprints.

Publisher's note Springer Nature remains neutral with regard to jurisdictional claims in published maps and institutional affiliations.

Open Access This article is licensed under a Creative Commons Attribution-NonCommercial-NoDerivatives 4.0 International License, which permits any non-commercial use, sharing, distribution and reproduction in any medium or format, as long as you give appropriate credit to the original author(s) and the source, provide a link to the Creative Commons licence, and indicate if you modified the licensed material. You do not have permission under this licence to share adapted material derived from this article or parts of it. The images or other third party material in this article are included in the article's Creative Commons licence, unless indicated otherwise in a credit line to the material. If material is not included in the article's Creative Commons licence and your intended use is not permitted by statutory regulation or exceeds the permitted use, you will need to obtain permission directly from the copyright holder. To view a copy of this licence, visit http://creativecommons.org/licenses/by-nc-nd/4.0/.

© The Author(s) 2026